Analyzing Longitudinal Magnetoresistance Asymmetry to Quantify Doping Gradients: Generalization of the van der Pauw Method

Wang Zhou, H. M. Yoo, S. Prabhu-Gaunkar, L. Tiemann, C. Reichl, W. Wegscheider, and M. Grayson

Generalized Van der Pauw Analysis for Quantifying Density Gradients from Asymmetric Longitudinal Magnetoresistance

Wang Zhou,[1] H. M. Yoo,[1] S. Prabhu-Gaunkar,[1] L. Tiemann,[2] C. Reichl,[2] W. Wegscheider,[2] and M. Grayson[1, *]

[1] Electrical Engineering and Computer Science, Northwestern University, Evanston, IL 60208, USA
[2] Laboratory for Solid State Physics, ETH Zürich, 8093 Zürich, Switzerland

A longitudinal magnetoresistance asymmetry (LMA) between positive versus negative magnetic field is known to occur in both the extreme quantum limit and the classical Drude limit in samples with non-uniform doping density. By analyzing the current stream-function in van der Pauw measurement geometry, it is shown that the electron density gradient can be quantitatively deduced from this LMA in the Drude regime. Results agree with gradients interpolated from local densities calibrated across an entire wafer, establishing a generalization of the van der Pauw method to quantify density gradients.

Experimental measurements of longitudinal magnetoresistance R_{xx} in semiconductor quantum wells (QWs) can show asymmetry with respect to positive and negative magnetic field B. At large fields and low temperatures in the quantum Hall (QH) regime, larger R_{xx} peaks appear for one sign of magnetic field, and smaller or vanishing R_{xx} peaks for the opposite field [1] obeying the Onsager-Casimir relations [2–4]. However, the underlying cause of the asymmetries remained unknown until more recent work by Pan *et al.* [5] in the fractional QH regime, whereby quantized R_{xx} maxima were explained by assuming an electron density difference across the sample. Motivated by this experiment, Ilan *et al.* [6] introduced a stream-function [7] model for current flow in the QH regime under an electron density gradient in the high-B limit $\rho_{xx} \ll \rho_{xy}$, and were able to explain the key features observed by Pan, where ρ_{xx} and ρ_{xy} are the longitudinal and transverse resistivities, respectively.

Despite the relevance of the above work, the low-magnetic field Drude limit, whereby resistivity components $\rho_{xx} \sim \rho_{xy}$ are of the same order, has a much broader practical scope than the restricted QH regime considered above. The majority of semiconductor characterizations are in this low-B limit, such as room temperature characterizations of samples with any mobility, and moderate-mobility magnetotransport of samples at any temperature. The above analysis of Ilan *et al.* also suffers from the significant drawback that it is not able to deduce the two independent components of the density gradient from a single sample. Yet density anisotropies are important to characterize since spurious effects in QH traces [1, 5] can result from wafer-scale density variations inherent to epitaxial growth [8], and inaccurate estimates of the activation energies of the QH regime are shown to result from anisotropic current flow [9]. Thus there remain significant challenges for magnetotransport characterization of inhomogeneously doped samples.

In this paper, the longitudinal magnetoresistance asymmetry (LMA) is comprehensively studied for an *arbitrarily* oriented density gradient in the more broadly
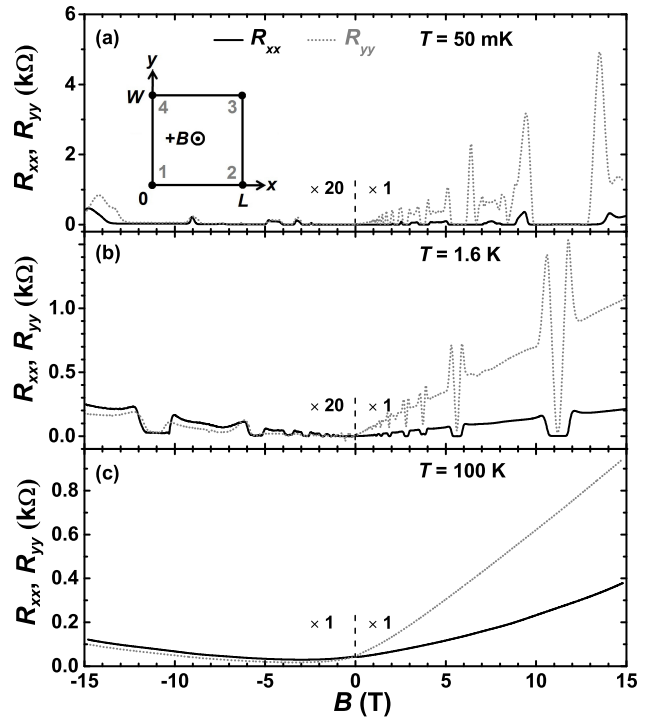

FIG. 1. Asymmetric longitudinal magnetoresistance $R_{xx} = R_{43,12}$ and $R_{yy} = R_{32,41}$ of sample D4 in the QH regime at (a) $T = 50$ mK, (b) 1.6 K, and in the Drude regime at (c) $T = 100$ K. The curves for $-B$ fields are magnified by 20 times for (a) and (b) in order to see subtle features. Note how the asymmetry exaggerates with decreasing temperature. Inset: Sample layout for a square sample $L = W$.

relevant low-magnetic field Drude limit for the first time, and a method to *quantitatively* measure both components of the density gradient is developed and calibrated against interpolated local densities of neighboring samples. Drastically asymmetric longitudinal resistance is observed in van der Pauw (vdP) samples [15] in both the QH and the Drude regime (Fig. 1). We find that

upon entering the Drude regime at higher temperatures, the LMA can be quantitatively explained with a model that assumes a density gradient in a classical Drude conductor. This LMA analysis deduces the magnitude and direction of the density gradient $\boldsymbol{\nabla} n$ as well as the local resistivity $\rho_0\,(B)$ from a consideration of 4-point resistances at both positive and negative B-fields. Such a technique promises to revolutionize magnetotransport characterization, allowing one to estimate density gradients with a simple extension of the vdP method [15]. We verify the validity and reproducibility of this LMA method on square samples cleaved from a high-mobility GaAs QW wafer. Both the angle and magnitude of the density gradients from this method match those interpolated from local electron density measurements.

Our experiments were carried out on a 2-inch wafer hosting a 30 nm-wide GaAs QW, with an average electron density $\bar{n} = 2.6 \times 10^{11}$ cm^{-2} and mobility $\bar{\mu} = 6.6 \times 10^6$ cm^2/V·s at $T = 1$ K. The wafer was grown by molecular beam epitaxy in a Gen II Varian chamber without any rotation during growth, leading to moderate density gradients as large as 20%/cm caused by the asymmetric positioning of the Ga, Al, and Si-dopant fluxes. The wafer was diced into 4×4 mm^2 square samples that were each contacted with four indium dots on the corners and four on the flats of each side, and then alloyed. Samples were measured in both a dilution refrigerator and ^{4}He flow cryostat ($T = 50$ mK - 300 K) with standard lock-in techniques.

Figure 1 shows the two longitudinal resistances $R_{xx} = R_{43,12}$ and $R_{yy} = R_{32,41}$ of sample D4 measured at $\pm B$-fields at $T = 50$ mK, 1.6 K and 100 K. The notation $R_{43,12}$ means current is sent from contact 4 to 3, and voltage is measured at contact 1 relative to 2 [15, 16]. According to the symmetry of the measurement, one would expect a perfectly homogeneous sample to exhibit the same longitudinal resistances R_{xx} and R_{yy} for $+B$ and $-B$-fields. However, at the lowest temperatures an extreme anisotropy is observed in the QH R_{xx} and R_{yy} traces (Fig. 1a), which decreases with increasing temperature (Fig. 1b), but still persists up to the Drude limit at $T = 100$ K (Fig. 1c). The analysis below will focus on this high temperature Drude regime where quantum oscillations vanish. To stay within the Drude limit, the temperature was kept above $T \geq 30$ K to suppress quantum oscillations and below $T \leq 100$ K to avoid parallel conduction in the doping layers.

To theoretically model the observed LMA, a rectangular sample (Fig. 1 insert) with a local density gradient is considered. The resistivities obey the local Drude equations $\rho_{xx}(\mathbf{r}) = {}^1\!/n(\mathbf{r})e\mu(\mathbf{r})$ and $\rho_{xy}(\mathbf{r}) = {}^B\!/n(\mathbf{r})e$, and a stream function ψ describes the current density $\mathbf{j}\,(\mathbf{r}) = \hat{\mathbf{z}} \times \nabla\psi\,(\mathbf{r})$ [7]. The local electric field $\mathbf{E}\,(\mathbf{r}) = \rho(\mathbf{r})\mathbf{j}(\mathbf{r})$ must satisfy $\nabla \times \mathbf{E} = 0$ in steady state, leading to

$$\rho_{xx}\nabla^2\psi + \nabla\rho_{xx} \cdot \nabla\psi - \hat{\mathbf{z}} \cdot (\nabla\psi \times \nabla\rho_{xy}) = 0. \quad (1)$$

We then solve Eq. (1) under more general conditions than previously considered: whereas Ref. [6] neglects $\nabla\rho_{xx}$ in Eq. (1) for the high mobility and high magnetic field limit, this term must be preserved for the general treatment derived here. And unlike Ref. [6], we consider a density gradient that can be oriented in an *arbitrary* direction.

The $\nabla\rho_{xx}$ and $\nabla\rho_{xy}$ gradients can be defined in terms of a normalized density gradient,

$$\boldsymbol{\eta} = (\eta_x, \eta_y) = \frac{\nabla n}{n_0}. \quad (2)$$

The local mobility is assumed to follow a power-law dependence on local density according to the standard screening assumption $\mu(\mathbf{r}) = \mu_0 \cdot (n(\mathbf{r})/n_0)^\gamma$, typically $0.5 < \gamma < 1.5$ [17–19]. The subscript "0" identifies local values at the center of the sample, whereby n_0 is the density, $\mu_0(B)$ the B-dependent mobility, and $\rho_0(B) = 1/n_0e\mu_0(B)$ the B-dependent Drude resistivity at the center of the sample. The resulting resistivity gradients to first-order in $\boldsymbol{\eta}$ become

$$\nabla\rho_{xx} = -\rho_0\,(1+\gamma)\,\boldsymbol{\eta}, \ \ \nabla\rho_{xy} = -\rho_0\mu_0 B\boldsymbol{\eta}. \quad (3)$$

Equation (1) is now evaluated keeping all derivative terms up to 1st order, and the four-point longitudinal resistance at finite B becomes,

$$R_{xx} = R_{43,12} = -\frac{\rho_0}{I} \int_{x_2}^{x_1} \left(-\frac{\partial\psi}{\partial y}\right)_{y=0} dx$$
$$= e^{W/2\xi_x} \sum_{m=1}^{\infty} \frac{2m^2\pi^2 L\rho_0\lambda_m}{\sinh\left(\frac{1}{2}\lambda_m W\right)} \frac{\left[1-(-1)^m\cosh(L/2\xi_y)\right]}{\left[(L/2\xi_y)^2+m^2\pi^2\right]^2}, \quad (4)$$

with length scale $\boldsymbol{\xi} = (\xi_x, \xi_y)$ defined in terms of the components of $\boldsymbol{\eta}$

$$\frac{1}{\xi_x} = -\mu_0 B\eta_x - (1+\gamma)\,\eta_y, \ \ \frac{1}{\xi_y} = -\mu_0 B\eta_y + (1+\gamma)\,\eta_x, \quad (5)$$

where

$$\lambda_m = \sqrt{\left[B^2\mu_0^2 + (1+\gamma)^2\right]\boldsymbol{\eta}^2 + 4m^2\pi^2/L^2}. \quad (6)$$

The analogous expression for $R_{yy} = R_{32,41}$ follows from the simple rotation transformation $x \to -y$, $y \to x$, $\xi_x \to -\xi_y$, $\xi_y \to \xi_x$, and $L \rightleftharpoons W$.

In this paper, we consider only physically reasonable density gradients across a roughly square sample ($W \sim L$), such that the percent of density variation δ across the sample defines a small parameter,

$$\delta = \frac{\Delta n}{n_0} = |\boldsymbol{\eta} \cdot (L\hat{x} + W\hat{y})|. \quad (7)$$

Here Δn represents the maximum change in density across the sample, and the relative accuracy of all expressions below are specified in terms of δ.

The first task is to identify the angle of the density gradient θ over the full range of B. Upon evaluating the ratio $R_{xx}(+B)/R_{xx}(-B)$ from Eq. (4), the B-symmetric component of the exponential prefactor cancels, as does the summation term which is approximately symmetric in B for small δ, leaving

$$\ln \frac{R_{xx}(+B)}{R_{xx}(-B)} = -W\eta_x \mu_0(B)\, B. \tag{8}$$

The corresponding expression for R_{yy} follows from the rotation transformation, and combined with Eq. (8) the density gradient angle θ becomes,

$$\tan\theta = \frac{\eta_y}{\eta_x} = -\frac{\ln \frac{R_{yy}(+B)}{R_{yy}(-B)}}{\ln \frac{R_{xx}(+B)}{R_{xx}(-B)}} \cdot \frac{W}{L}, \tag{9}$$

accurate to within an error of less than $\frac{1}{2}\delta$.

To test Eq. (9), we independently estimate a density gradient angle θ_{int} interpolated from the densities of neighboring samples. Figure 2a compares the interpolated result $\theta_{\text{int}} = 117°$ to θ from the LMA method of Eq. (9). The gradient angle θ compares favorably and is constant at $114°$ over the entire range except for the lowest magnetic fields.

The second task is to determine $\rho_0(B)$, the B-dependent local resistivity, in the low B limit. From Eq. (6) and its rotation transform, λ_m is independent of magnetic field below $B'_x = 1/\mu_0|\eta_x|W$ and $B'_y = 1/\mu_0|\eta_y|L$. Therefore $B \leq B' = \min\{B'_x, B'_y\}$ sets the range where the approximation $\lambda_m \approx 2m\pi/L$ is valid [20], simplifying Equation (4),

$$R_{xx}(B) = e^{W/2\xi_x} \rho_0(B) \frac{16}{\pi}\Big[\tanh^{-1}\Big(e^{-\pi\frac{W}{L}}\Big) \\ + \sinh^2(L/4\xi_y)\cdot\ln\Big(1+e^{-\pi\frac{W}{L}}\Big)\Big]. \tag{10}$$

Equation (8) and its rotation transform along with Eq. (5) define $\boldsymbol{\eta}$ and $\boldsymbol{\xi}$, in turn. Substituting into Eq. (10) and solving for ρ_0 gives an expression for the resistivity which we label ρ_0^a,

$$\rho_0^a(B) = \sqrt{R_{xx}(+B)\,R_{xx}(-B)} \cdot \frac{\pi}{16}\Big[\tanh^{-1}\Big(e^{-\pi\frac{W}{L}}\Big)$$

$$+ \sinh^2\Big(\ln\frac{R_{yy}(+B)}{R_{yy}(-B)}/4\Big)\ln\Big(1+e^{-\pi\frac{W}{L}}\Big)\Big]^{-1}. \tag{11}$$

The rotation transformed Eq. (11) is labelled ρ_0^b, and the most accurate estimate of $\rho_0(B)$ is their average,

$$\rho_0(B) = \frac{1}{2}\big[\rho_0^a(B) + \rho_0^b(B)\big], \tag{12}$$

accurate to within δ.

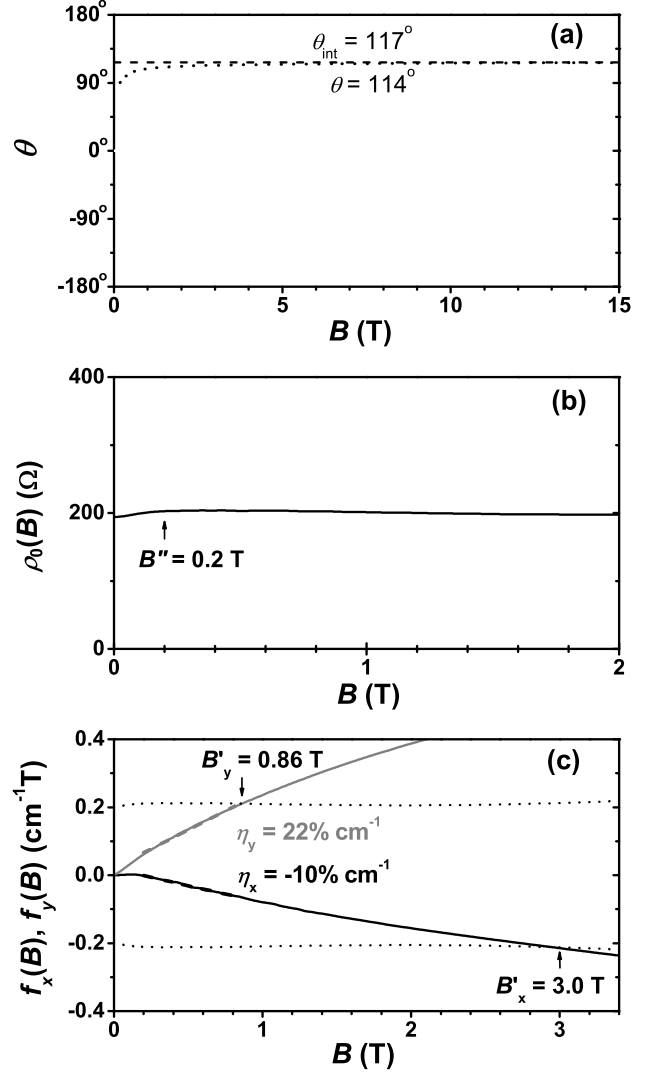Equations (11) and (12) generalize the classic van der Pauw equations [15] for the case of a density gradient.

FIG. 2. Gradient angle θ, resistivity ρ_0, and gradient parameters f_x and f_y are plotted as a function of B for sample D4. (a) The dotted line θ is constant $114°$ except at the lowest B, and compares favorably to the dashed line $\theta_{\text{int}} = 117°$ interpolated from neighboring samples. (b) $\rho_0(B)$ exhibits flat Drude behavior everywhere except below $B'' = 0.2$ T. (c) Normalized density gradient components η_x and η_y determined from the slopes of the linear fitting lines of $f_x(B)$ and $f_y(B)$ within $B'' < B < B'$.

The four contacted corners of the sample can all have different local resistivity and density, yet these equations can still estimate the local resistivity in the center of a sample $\rho_0(B)$. The result is plotted in Fig. 2b for sample D4, showing a Drude-like response with very little dependence on B except near $B = 0$ T where quantum phase coherent effects such as weak localization [21–23] and memory effects [24–27] as well as electron-electron interactions [28, 29] may play a role. We will there-
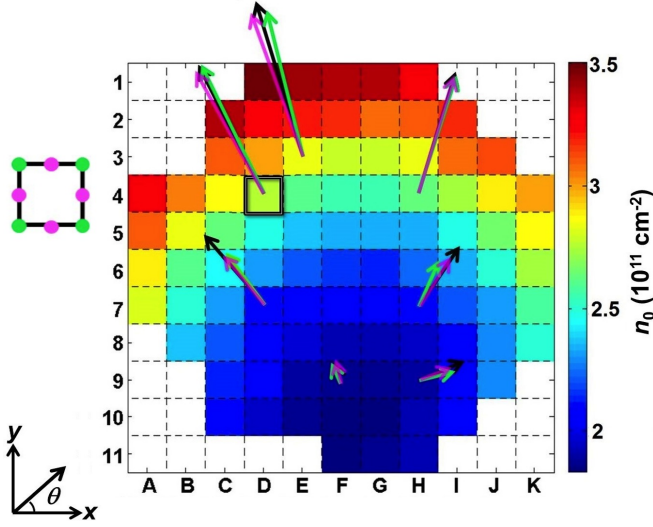
FIG. 3. Density color map of 2-inch GaAs QW wafer calibrated by dicing into 4×4 mm^2 samples and measuring the local density n_0 of various samples. Black arrows represent local density gradients $\boldsymbol{\nabla} n_{\rm int} = n_0 \boldsymbol{\eta}_{\rm int}$ interpolated from this density map. Green (pink) arrows represent LMA method density gradients $\boldsymbol{\nabla} n = n_0 \boldsymbol{\eta}$ using corner (flat) contacts. Sample D4 is presented in greater detail (Figs. 1 and 2).

fore identify a lower limit for Drude-like behavior as B'', which for sample D4 is $B'' = 0.2$ T.

The final task is to deduce the components of the density gradient from the low-B data. Multiplying Eq. (8) and its rotated counterpart on both sides by $\rho_0(B)$ yields the functions:

$$f_x(B) = -\frac{n_0 e}{W} \rho_0(B) \cdot \ln \frac{R_{xx}(+B)}{R_{xx}(-B)} = \eta_x B,$$
$$f_y(B) = \frac{n_0 e}{L} \rho_0(B) \cdot \ln \frac{R_{yy}(+B)}{R_{yy}(-B)} = \eta_y B. \tag{13}$$

Their slopes in B give the normalized density gradient,

$$\nabla n/n_0 = \boldsymbol{\eta} = \left(\frac{df_x}{dB}, \frac{df_y}{dB} \right). \tag{14}$$

In a perfect Drude model, these slopes would persist to $B = 0$ T, but since B'' sets the lower limit of the Drude behavior we only expect a linear fit within the domain $B'' < B < B'$.

Figure 2c illustrates how the density gradient can be deduced graphically. The functions $f_x(B)$ and $f_y(B)$ are plotted along with $1/\mu_0(B)L$ and $-1/\mu_0(B)W$. The condition for $B'_x = 1/\mu_0|\eta_x|W$ and $B'_y = 1/\mu_0|\eta_y|L$ is graphically determined from their intersection, and the low-B delimiter B' is identified with the lesser of B'_x or B'_y. From Fig. 2c, the density gradient components $\eta_x = -10\%$ cm^{-1} and $\eta_y = 22\%$ cm^{-1} are then extracted from the slopes of the linear fitting lines within the domain $B'' < B < B'$.

We can verify this LMA analysis across an entire wafer by creating an interpolated density map. The wafer is illustrated in Fig. 3 with various colored tiles designating the local measured densities. The interpolated normalized density gradients $\boldsymbol{\eta}_{\rm int} = \frac{\boldsymbol{\nabla} n_{\rm int}}{n_0}$ were deduced by calculating the first derivative of the density map smoothed via the so-called QR algorithm [30]. In addition to D4, six other samples marked with origins of each arrow in Fig. 3 were selected, and density gradients $\boldsymbol{\nabla} n_{\rm int}$ deduced from the interpolated data are plotted as black arrows. For comparison, the density gradient magnitudes and angles for these same samples were also determined with the LMA method, and $\boldsymbol{\nabla} n = n_0 \boldsymbol{\eta}$ is plotted with green arrows. Conformal equivalence [31, 32] also allows us to use four flat contacts at the center of each side to measure the density gradient, provided we rotate the resulting angle by 45°, with the result plotted in Fig. 3 as the pink arrows. The overlap of these gradient vectors verifies the consistency of the LMA method for calibrating density gradients.

As Fig. 3 demonstrates, the LMA analysis has the practical consequence of providing a quick and simple evaluation of density gradients of 2D conducting layers of single samples, in contrast to the cumbersome task of measuring the densities and mobilites of neighboring samples. To measure high-mobility samples such as those investigated here, higher temperatures are needed to increase the resistivity ρ_0 and thereby increase B' so that a wider range of B-field can be used to extract the density gradient magnitude.

To summarize, we observed an asymmetry in the longitudinal resistance in the QH and Drude regimes, and developed an analytical model to extract the density gradient. Equations (9) and (11)-(14) are unique to this work, and allow one to calculate the angle and magnitude of the density gradient, as well as the local resistivity $\rho_0(B)$, from the longitudinal resistances R_{xx} and R_{yy} in both $+B$ and $-B$ fields. The physics discussed here allows one to quantify uniformity of 2D materials such as graphene [33, 34], MoS$_2$ [35–37], WS$_2$ [38], β-metallic phosphorus [39], and topological insulators (TI) [40, 41], where individual micron-sized exfoliated samples do not have the luxury of having "neighboring" pieces to deduce density gradients. This work generalizes the classic vdP analysis to handle the case of a density gradient.

---

* m-grayson@northwestern.edu.

[1] F. Fischer, M. Grayson, E. Schuberth, D. Schuh, M. Bichler, and G. Abstreiter, Physica E **22**, 108 (2004).
[2] L. Onsager, Phys. Rev. **38**, 2265 (1931).
[3] H. B. G. Casimir, Rev. Mod. Phys. **17**, 343 (1945).
[4] H. H. Sample, W. J. Bruno, S. B. Sample, and E. K. Sichel, J. Appl. Phys. **61**, 1079 (1987).
[5] W. Pan, J. S. Xia, H. L. Stormer, D. C. Tsui, C. L. Vicente, E. D. Adams, N. S. Sullivan, L. N. Pfeiffer, K. W. Baldwin, and K. W. West, Phys. Rev. Lett. **95**, 066808 (2005).
[6] R. Ilan, N. R. Cooper, and A. Stern, Phys. Rev. B **73**, 235333 (2006).
[7] I. M. Ruzin, N. R. Cooper, and B. I. Halperin, Phys. Rev. B **53**, 1558 (1996).
[8] L. N. Pfeiffer and K. W. West, private correspondence , (2014).
[9] J. P. Eisenstein, preprint , (2014).
[10] M. A. Zudov, R. R. Du, L. N. Pfeiffer, and K. W. West, Phys. Rev. Lett. **90**, 046807 (2003).
[11] R. G. Mani, Phys. Rev. B **72**, 075327 (2005).
[12] R. R. Du, H. L. Stormer, D. C. Tsui, L. N. Pfeiffer, and K. W. West, Phys. Rev. Lett. **70**, 2944 (1993).
[13] J. Huang, L. N. Pfeiffer, and K. W. West, Phys. Rev. Lett. **112**, 036803 (2014).
[14] M. P. Lilly, J. L. Reno, J. A. Simmons, I. B. Spielman, J. P. Eisenstein, L. N. Pfeiffer, K. W. West, E. H. Hwang, and S. DasSarma, Phys. Rev. Lett. **90**, 056806 (2003).
[15] L. J. van der Pauw, Philips Research Reports **13**, 1 (1958).
[16] B. S. Kim, W. Zhou, Y. D. Shah, C. Zhou, N. Isik, and M. Grayson, Rev. Sci. Instrum. **83**, 024703 (2012).
[17] L. Pfeiffer, K. W. West, H. L. Stormer, and K. W. Baldwin, Appl. Phys. Lett. **55**, 1888 (1989).
[18] B. E. Kane, L. N. Pfeiffer, K. W. West, and C. K. Harnett, Appl. Phys. Lett. **63**, 2132 (1993).
[19] K. Hirakawa and H. Sakaki, Phys. Rev. B **33**, 8291 (1986).
[20] This case is more likely to occur in smaller samples or at higher resistivities ρ_0, which can be found at higher temperatures in high mobility samples such as the ones studied here.
[21] E. McCann, K. Kechedzhi, V. I. Falko, H. Suzuura, T. Ando, and B. L. Altshuler, Phys. Rev. Lett. **97**, 146805 (2006).
[22] T. Hassenkam, S. Pedersen, K. Baklanov, A. Kristensen, C. B. Sorensen, P. E. Lindelof, F. G. Pikus, and G. E. Pikus, Phys. Rev. B **55**, 9298 (1997).
[23] L. Bockhorn, P. Barthold, D. Schuh, W. Wegscheider, and R. J. Haug, Phys. Rev. B **83**, 113301 (2011).
[24] E. M. Baskin and M. V. Entin, Physica B **249**, 805 (1998).
[25] A. D. Mirlin, J. Wilke, F. Evers, D. G. Polyakov, and P. Wolfle, Phys. Rev. Lett. **83**, 2801 (1999).
[26] A. Dmitriev, M. Dyakonov, and R. Jullien, Phys. Rev. Lett. **89**, 266804 (2002).
[27] L. Bockhorn, I. V. Gornyi, D. Schuh, C. Reichl, W. Wegscheider, and R. J. Haug, Phys. Rev. B **90**, 165434 (2014).
[28] I. V. Gornyi and A. D. Mirlin, Phys. Rev. B **69**, 045313 (2004).
[29] E. A. Galaktionov, A. K. Savchenko, and D. A. Ritchie, Phys. Status Solidi C **3**, 304 (2006).
[30] J. G. F. Francis, The Computer Journal **4**, 265 (1961).
[31] L. V. Bewley, *Two-dimensional fields in electrical engineering* (Macmillan Co., New York, 1948).
[32] N. Zeev, *Conformal Mapping* (Dove, New York, 1975).
[33] B. Ozyilmaz, P. Jarillo-Herrero, D. Efetov, D. A. Abanin, L. S. Levitov, and P. Kim, Phys. Rev. Lett. **99**, 166804 (2007).
[34] J. Jobst, D. Waldmann, I. V. Gornyi, A. D. Mirlin, and H. B. Weber, Phys. Rev. Lett. **108**, 106601 (2012).
[35] B. Radisavljevic, A. Radenovic, J. Brivio, V. Giacometti, and A. Kis, Nature Nanotech. **6**, 147 (2011).
[36] K. F. Mak, C. Lee, J. Hone, J. Shan, and T. F. Heinz, Phys. Rev. Lett. **105**, 136805 (2010).
[37] D. Xiao, G.-B. Liu, W. Feng, X. Xu, and W. Yao, Phys. Rev. Lett. **108**, 196802 (2012).
[38] H. S. S. R. Matte, A. Gomathi, A. K. Manna, D. J. Late, R. Datta, S. K. Pati, and C. N. R. Rao, Angew. Chem. and Int. Ed. **49**, 4059 (2010).
[39] L. Li, Y. Yu, G. J. Ye, Q. Ge, X. Ou, H. Wu, D. Feng, X. H. Chen, and Y. Zhang, Nature Nanotech. **9**, 372 (2014).
[40] N. Bansal, Y. S. Kim, M. Brahlek, E. Edrey, and S. Oh, Phys. Rev. Lett. **109**, 116804 (2012).
[41] K. Nomura and N. Nagaosa, Phys. Rev. Lett. **106**, 166802 (2011).